



Environmental
Science
Nano

Nanoplastics Prepared with Uniformly Distributed Metal-tags: A Novel Approach to Quantify Size Distribution and Particle Number Concentration of Polydisperse Nanoplastics by Single Particle ICP-MS

Journal:	<i>Environmental Science: Nano</i>
Manuscript ID	EN-ART-05-2023-000342.R1
Article Type:	Paper

SCHOLARONE™
Manuscripts

1
2
3
4
5
6
7
8
9
10
11
12
13
14
15
16
17
18
19
20
21
22
23
24
25
26
27

Nanoplastics Prepared with Uniformly Distributed Metal- tags: A Novel Approach to Quantify Size Distribution and Particle Number Concentration of Polydisperse Nanoplastics by Single Particle ICP-MS

28 Casey Smith^{1,*}, Stephanie Brown^{1,*}, Nathan Malone^{1,*}, Shaun Bevers², James Ranville², D.
29 Howard Fairbrother¹
30

31
32
33 ¹Department of Chemistry, Johns Hopkins University, Baltimore, MD 21218, United States
34

35 ²Department of Chemistry, Colorado School of Mines, Golden, CO 80401, United States
36
37

38 *C.S., S.B., and N.M contributed equally to this work.
39
40
41
42
43
44
45
46
47
48
49
50
51
52
53
54
55
56
57
58
59
60

Abstract

Nanoplastics (NPs, $< 1 \mu\text{m}$), the smallest size fraction of environmental microplastics, are a contaminant of emerging concern due their high environmental concentrations, enhanced environmental mobility, and greater bioavailability compared to microplastics. Due to their majority carbon composition, diversity in size, polymer type, surface properties, and shape, NPs are difficult to detect and quantify, hindering our ability to understand NP behavior. To overcome this challenge, we have created irregularly shaped metal-tagged NPs with continuous sub-micron size distributions by cryo-milling lab-generated plastics containing 1% w/w concentrations of an organometallic additive. These metal-tagged NPs are detectable by single particle ICP-MS (spICP-MS) which is capable of measuring NP size distributions (PSD) and particle numbers (PNC) at low μgL^{-1} concentrations. The ease of synthesis and flexibility of this method has enabled a suite of metal-tagged NPs to be created for a range of commercially important polymers (PS, PMMA, PVC, LDPE, PVP). By using unique metal additive-polymer combinations (e.g. PS tagged with Sn, PMMA tagged with Ta) the influence of polymer composition on NP environmental behavior can be studied using NP mixtures. Due to the sensitivity of the spICP-MS, we are able to use low metal-loadings to ensure the NPs surface properties remain unchanged compared to unmodified NPs. Advantages of this approach compared to existing NP labelling approaches are discussed along with illustrative examples in laboratory-based studies of NP production from macroscopic plastics (e.g. abrasion), photochemical NP degradation, and NP uptake into biological organisms.

Environmental Significance

Chemical (e.g. photolysis) or physical (e.g. abrasion) processes degrade discarded plastics over time into vast numbers of nanoplastics (NPs). Despite a dominance by number and likely importance in determining environmental impacts of plastics, significant analytical challenges have prevented detection and quantification of NPs. We have created metal-tagged NPs with irregular shapes, diverse sizes, and multiple polymer compositions. We demonstrate measurement of particle number concentration (PNC) and particle size distribution (PSD) in complex, heterogeneous matrices at low μgL^{-1} concentrations. This new methodology will facilitate lab-based studies designed to elucidate the behavior and impact of these NPs in aquatic and terrestrial environments as well as the PNC and PSD of NPs released from polymers during chemical and physical processes.

Introduction

Since the 1950s, the production and accumulation of plastics has dramatically increased but only 21% of the cumulative 6500 million metric tons produced by 2015 has been recycled or incinerated.¹ Due to the minimal chemical and biological degradation of most polymers, the remaining portion of plastics has accumulated in landfills or natural environments and generated an estimated 3 million metric tons of microplastics (MPs).² In the past decade, public concern has shifted from macroscopic plastic debris to these MPs³, typically defined as < 5 mm in diameter.⁴⁻
⁸ The observation of MPs in various marine organisms in coastal sediment, soil environments, and drinking water sources such as freshwater lakes, rivers, and reservoirs⁹⁻¹¹ confirms ingestion as a key route of MP exposure in multiple ecosystems. Additionally, if ingested MPs are transferred from prey to predators, there is a risk for further accumulation at higher trophic levels.¹² This could be an issue for human health if MP accumulation occurs in marine species consumed by humans.¹³⁻
¹⁶ The uptake of MPs by edible plants is also a public health and food security issue,¹⁷ and consumption of MPs through ingestion of particle-containing food has been cited as a threat to global food security and human health.

MPs that enter the environment originate from two sources: primary or secondary MPs. Primary MPs are plastics intentionally designed with microscale sizes, such as microbeads in cosmetics or microfibers from textiles. Secondary MPs are derived from larger plastic products (e.g. fishing nets, containers, etc.) that progressively fragment into smaller particles due to natural weathering processes, including photochemical, physical, and biological degradation.¹⁸⁻²¹ Given the variety of possible ways in which they can be produced, MPs exhibit heterogeneous morphology, chemical composition, and size.

1
2
3 The fraction of MPs with the smallest sizes ($< 1 \mu\text{m}$) can be separately classified as
4 nanoplastics (NP). Much of the recent literature has used micro(nano)plastics (MnP) to combine
5 both size classes, but this terminology does not acknowledge their very different size regimes and
6 behaviors.²² *Herein, when specifically discussing plastics with sizes $< 1 \mu\text{m}$ we will utilize the*
7 *term NP.* A focus on NP behavior is warranted because health hazards will likely be greater for
8 NPs because decreasing size results in an increasing surface-area-to-volume ratio, potential for
9 transport, and facilitated-transport of sorbed contaminants in marine environments.²³⁻²⁵ Moreover,
10 for the polydisperse particles present in the environment, particle number concentrations increase
11 exponentially as particle size decreases.²⁶ Consequently, organism exposure is greater for smaller
12 NPs compared to MPs.²⁷ If uptake occurs, NPs have also been shown capable of eliciting persistent
13 immune and oxidative stress responses that can lead to physiological changes such chronic
14 inflammation and tissue damage.²⁸⁻³³ Moreover, in drinking water treatment, because particle
15 removal rates generally decrease with decreasing particle size, smaller sized MPs and NPs are of
16 more concern for public health.³⁴⁻³⁶ With plastic production estimated to increase 5-fold by 2050¹
17 and growing evidence of the detrimental health impacts of NPs, developing a fundamental
18 understanding of the behavior and properties of NPs is therefore imperative.

19
20
21
22
23
24
25
26
27
28
29
30
31
32
33
34
35
36
37
38
39
40 One significant obstacle in studying NP behavior in natural environments is the inherent
41 challenge in their collection, detection, and quantification. Primary difficulties include obtaining
42 a sufficient number of NPs to allow analysis and distinguishing these plastic particles from
43 naturally occurring, carbon-based particles (e.g. cells, detritus). In principle, NPs could be
44 fractionated and concentrated separately from background particles by means such as density
45 separation, sieving, and selective digestion of sediment particles with peroxide. However, these
46 preparatory steps can influence the final size and surface properties of the NPs.^{37, 38} Incomplete
47
48
49
50
51
52
53
54
55
56
57
58
59
60

1
2
3 removal of extraneous material results in the presence of background particles in the sub-micron
4 size range, which leads to an overestimate of NPs in the sample.³⁷ A few high resolution separation
5 techniques (e.g. field flow fractionation) are capable of discriminating NPs from some natural
6 environmental constituents (e.g. NOM), although these methods have yet to find widespread
7 implementation.^{39, 40}

8
9
10
11
12
13
14
15 Even if NPs can be successfully separated from interfering natural particles, identifying
16 their chemical composition, determining their physicochemical properties (e.g. size), and
17 quantifying their concentration, are acutely difficult for all but the most pristine samples.^{41, 42}
18
19 Laser-based sizing techniques, such as dynamic light scattering (DLS), can measure NP particle
20 size distribution (PSD) but not concentration (PNC, # of particles per mL), and nanoparticle
21 tracking analysis (NTA), which can provide both PSD and PNC, is limited to sub-micron sizes.
22
23 The inability of NTA and DLS to differentiate NPs from background particles also prevents their
24 use for most environmental matrices.^{43, 44} In principle PSD and PNC of NPs is possible by using
25 single particle ICP-MS (spICP-MS) analysis using ¹³C.⁴⁵ This less abundant isotope of carbon
26 (1.16%) is used to avoid the high natural ¹²C background ICP-MS signal generated by the
27 ubiquitous presence of carbon dioxide. However, the high ionization potential of carbon (11.26
28 eV), which causes a low (< 5%) ionization efficiency in the plasma, combined with high carbon
29 background functionally limits ¹³C spICP-MS analysis to sizes above 1.5-2 micron for PS.⁴⁵
30
31 Furthermore, the use of ¹³C for NP quantification in complex environmental samples where
32 carbon-containing particles are present is not possible. Electron microscopy (EM) techniques such
33 as scanning electron microscopy (SEM) and transmission electron microscopy (TEM) are capable
34 of measuring PSDs at micro- and nanoscale dimensions, respectively, but similarly cannot easily
35 distinguish NPs from other carbon-based particles. With EM, there is also great difficulty
36
37
38
39
40
41
42
43
44
45
46
47
48
49
50
51
52
53
54
55
56
57
58
59
60

1
2
3 translating the particle numbers observed in each image to the aqueous PNC in the original
4 sample.⁴⁶ EM is also a low-throughput technique and drying effects during sample preparation
5
6 may cause unwanted particle aggregation leading to PSD distortion.
7
8
9

10 The numerous issues associated with the collection, detection, and quantification of NPs
11 in the natural environment provide the impetus to generate NPs specifically for the purpose of
12 laboratory-based studies. Researchers often use readily available, commercially synthesized
13 materials to study NP behavior,⁴⁷ but with several drawbacks. For example, the surfaces are often
14 modified with surfactants to facilitate dispersion and the NPs are produced as monodisperse
15 spheres. This makes commercially synthesized NPs a poor proxy for the irregularly shaped and
16 polydisperse NPs found in natural environments. Furthermore, the range of polymers
17 commercially available as NPs is extremely limited (typically only polystyrene and poly(methyl
18 methacrylate)). The alternative for researchers is to create NPs in house. NPs can be synthesized
19 bottom-up via polymerization,⁴⁸⁻⁵¹ but the synthesis process limits their resultant heterogeneity in
20 polymer type, size, shape, and surface morphology.⁴⁷ In contrast, NPs can be created top-down
21 from bulk polymers through laboratory weathering, accomplished through a combination of UV
22 exposure and mechanical abrasion,⁵² sonication-based fragmentation,^{53, 54} or from cryogenic
23 milling.^{55, 56} A key advantage of these top-down methods is the ability to recreate the heterogeneity
24 in size, shape, and surface morphology of NPs generated from plastic waste under environmental
25 conditions.⁵⁷ However, without the inclusion of a tracer, these NPs cannot be sized, quantified, or
26 tracked in complex, realistic environmental matrices. This is due primarily to the inability of most
27 analysis methods to differentiate NPs from other carbon-containing “background” particles, clays
28 and other naturally occurring submicron particles, which are likely present at much higher
29
30
31
32
33
34
35
36
37
38
39
40
41
42
43
44
45
46
47
48
49
50
51
52
53
54
55
56
57
58
59
60

1
2
3 concentrations. This severely limits the use of model NPs in laboratory studies designed to study
4
5 their environmental behavior (e.g. biological uptake or transport studies).
6

7
8 To overcome these issues, NPs modified by the addition of identifiable tracers, specifically
9
10 fluorophores or metals, have been synthesized and employed.^{38, 58-60} These labelling approaches
11
12 render the NPs distinguishable from other background particles with use of an appropriate
13
14 analytical technique.^{61, 62} The use of fluorophores is, however, generally used to quantitatively
15
16 determine NP uptake or track their movements using techniques such as imaging by fluorescence
17
18 microscopy.^{38, 63, 64} In contrast, the analysis of metal tagged NPs by ICP-MS provides quantitative
19
20 NP mass concentrations but no information on PSD or PNC.
21
22

23
24 In this paper, we present a new labelling approach which involves the top-down synthesis
25
26 of irregularly-shaped, polydisperse NPs which contain uniform concentrations of embedded (i.e.
27
28 tagged) organometallic additives. Incorporating organometallic compounds at a low loading (1%
29
30 w/w) does not alter the bulk or surface properties of the NPs and enables spICP-MS measurement
31
32 to determine PNC and PSD for a range of commercially important NPs (including PS, PMMA,
33
34 PVC, LDPE, PVP) in complex matrices. Cryomilling creates NPs whose PSDs span the full
35
36 submicron range, with the greatest number occurring at the very smallest sizes. This new
37
38 methodology can be easily implemented in different research laboratories having ICP-MS
39
40 capabilities. Furthermore, we provide several example environmental applications to demonstrate
41
42 suitability of the approach to NP analysis.
43
44
45
46
47
48
49
50
51
52
53
54
55
56
57
58
59
60

Materials and methods

Selection of plastics and organometallic additives

Given the broad range of polymers used to manufacture plastics, we demonstrated the general utility of our approach by preparing metal-tagged NPs using five commercially available polymers with varying chemical characteristics. These polymers have also been previously detected as MPs in relatively high quantities in a range of natural environments.⁶⁵⁻⁶⁷ (1) Polystyrene (PS) a hydrophobic polymer, found in packaging, containers, lids, bottles and trays; (2) Low density polyethylene (LDPE), a hydrophobic plastic used to make containers, plastic bottle tops and packaging; (3) Polyvinyl chloride (PVC), used to make pipes, non-food packaging, and plastic cards; (4) Polymethyl methacrylate (PMMA), a hydrophilic polymer used in cell phone screens and as a substitute for glass in lenses; (5) Polyvinylpyrrolidone (PVP), a hydrophilic polymer which, along with LDPE and PMMA, has been used as plastic microbeads in cosmetics. Organometallic complexes were selected as the metal-tag source (e.g Ta, Sn, and Zr) based on the following criteria: (i) solubility in a volatile organic solvent also capable of dissolving the selected polymer, (ii) the metal's sensitivity for detection by spICP-MS, and (iii) the metal's low abundance in the environment, thereby facilitating discrimination of the metal-tagged NPs from background signals (e.g. clays containing metals such as Al, Fe, Si, Ti).

All chemicals were used as received without further purification. All organic solvents used were ACS reagent grade. Poly(methyl methacrylate) (MW=168,000), polystyrene (MW=280,000), polyvinylchloride (MW=35,000), polyvinylpyrrolidone (MW=10,000), and low-density polyethylene (MW=4,000) were purchased from Sigma Aldrich. Organometallic complexes tantalum (V) ethoxide, tantalum (V) chloride, zirconium (IV) ethoxide, and platinum

1
2
3 2,4-pentanedionate were purchased from Alfa Aesar. Dibutyltin diacetate was purchased from TCI
4
5 Chemicals.
6
7
8
9

10 **Synthesis of metal-tagged plastics**

11
12 Metal tags were incorporated into each of the polymers via solution blending^{68, 69} where
13
14 mixture of organometallic additive and polymer are sonicated in an organic co-solvent. Solution
15
16 blending was preferred over melt mixing/extrusion to optimize uniformity of additive dispersion
17
18 within the polymer, an important attribute in determining NP size distribution.^{70, 71} All % w/w
19
20 values herein refer to the mass loading of organometallic additive with respect to mass of polymer.
21
22 Unless otherwise noted, a 1% w/w additive loading was used to create the casting solution. Once
23
24 both additive and polymer were visibly dissolved, the blended solution was poured into an
25
26 aluminum dish (12.7 cm, Juvalé, Amazon), and the solvent subsequently volatilized at room
27
28 temperature for approximately 48 hours (Figure SI-1). To ensure full solvent removal from the
29
30 material, the composite was dried under vacuum at 35°C for an additional 48 hours. All composites
31
32 were then recovered from the aluminum dishes and trimmed to a uniform size, approximately 9
33
34 cm diameter. The mass of polymer and metal additive used are gravimetrically determined during
35
36 synthesis. Given that the polymers and the additives are involatile and there is no material loss
37
38 during solution blending except for solvent evaporation, the metal content in the polymers can be
39
40 assumed to be well determined.
41
42
43
44
45
46

47 A schematic of the solution blending process demonstrating the preparation of PS
48
49 containing Sn and PMMA containing Ta using chloroform and benzene, respectively, as co-
50
51 solvents is shown in Figure 1. Table A describes the organometallic additive, polymer, and solvent
52
53
54
55
56
57
58
59
60

1
2
3 combinations utilized to create metal-tagged NPs to-date. Further detail regarding each composite
4
5 synthesis (reagent masses, solvent volume, and sonication time) can be found in Table SI-1.
6

7 **Generation and characterization of metal-tagged nanoplastics**

8
9
10 Metal-tagged composites were cut into approximately 1 x 1 cm² pieces for milling in
11
12 polycarbonate cryomill tubes with a stainless-steel impactor and end caps (Spex 6700
13
14 Freezer/Mill). Composites were cooled with liquid nitrogen and milled for a total of 30 minutes
15
16 (6, 5-minute cycles) at an impact frequency of 15 Hz with a 2-minute cool period between
17
18 cycles. This process served as an accelerated form of mechanical erosion/fracturing and generated
19
20 irregularly shaped NPs that contained a broad range of particle sizes, from nanometer to micron
21
22 (Figure 1).
23
24

25
26 The physiochemical properties of the metal-tagged plastics were determined using a
27
28 combination of attenuated total reflectance-infrared spectroscopy (ATR-IR), differential scanning
29
30 calorimetry (DSC), water contact angle measurement, and X-ray photoelectron spectroscopy
31
32 (XPS). All data were acquired on the cryomilled powders, except for the water contact angle
33
34 measurements which used the as-prepared composites. Additionally, μ -X-ray Fluorescence (μ -
35
36 XRF) mapping of the metal-tagged plastics (M4 TORNADO u-XRF (Bruker)) was used to
37
38 determine the distribution of metal additive within the plastic composites. Further details on data
39
40 collection and analysis are provided in the SI.
41
42
43

44 **Preparation of water-stable nanoplastic suspensions**

45
46
47 Cryomilled plastic particles were added to deionized water at a concentration of 1 mg/mL
48
49 and sonicated in an ice water bath (Branson 1510 ultrasonicator bath, Danbury, CT) for 24 hours.
50
51 After sonication, the solution was allowed to settle undisturbed for another 24 hours in an
52
53 Erlenmeyer flask. The supernatant was then removed from approx. 0.5 cm below the surface to
54
55
56
57
58
59
60

1
2
3 approx. 0.5 cm above the bottom of the flask to collect only those particles that remained in
4 suspension. The degree to which different NPs formed stable suspensions depended on the
5 polymer type. To determine suspension efficiency, a known volume of the isolated supernatant
6 was lyophilized and mass of suspended microplastics measured. 100% of PVP, a water-soluble
7 polymer formed stable colloidal NPs at a mass loading of 1 mg/mL. For the other polymers tested,
8 lower fractions of the initial 1 mg/mL suspension remained stable. Specifically, suspension
9 efficiencies for PMMA, LDPE, and PS were 13.7%, 8.8%, and 5.9%, broadly in line with their
10 respective hydrophilicities.⁷²

21 **Quantification and sizing of metal-tagged nanoplastics**

22
23
24 Single particle optical sensing analysis (SPOS) (Particle Sizing Systems – SNS 760) was
25 used to characterize the number and size distribution of NPs in the size range of 0.5-500 μm . The
26 SPOS software combined the data from an extinction sensor (180° angle) and a scattering sensor
27 (135° angle). Additionally, SEM (JEOL, JSM-IT100) was used to assess the surface morphology
28 and size of nanoplastics.

29
30
31 The principal method used for size characterization of the metal-tagged nanoplastics was
32 spICP-MS (Perkin Elmer NexION 300 D) analysis of water-stable NP suspensions. As discussed
33 in the introduction, spICP-MS is uniquely well suited to quantify PSDs and PNCs of metal-tagged
34 NPs (schematic workflow is shown in Figure 2). NPs were analyzed for ^{181}Ta , ^{118}Sn , and ^{90}Zr .
35 Suspensions were introduced into the plasma using a Meinhard nebulizer (ESI, Golden CO) and a
36 cyclonic spray chamber (PerkinElmer, Waltham, MA). Each time a metal-tagged NP enters the ICP
37 plasma it is vaporized, generating a discrete plume of metal ions that are mass-selected by a
38 quadrupole and registered as a pulse in the detector's time resolved output. These particle
39 generated pulses are registered when the signal exceeds a threshold value,⁷³ which is typically set

1
2
3 as the mean of all background signals plus three times the standard deviation ($\mu + 3\sigma$). In a 60
4 second analysis using 100 μ s dwell times, it is typical to measure on the order of 1000-10,000
5 particles. The size-based method⁷⁴ was used to determine transport efficiency (TE), which ranged
6 from 5-8 % throughout the study.
7
8
9
10

11
12 After accounting for TE, NPs can be sized and counted using the metal mass detected in
13 each individual NP. Assuming a uniform distribution of metals in the plastic, the intensity of each
14 pulse measures the NP effective size/diameter through:
15
16
17

$$18 \quad NP \text{ Volume } (V) = \text{Sum of Pulse Intensities} \times \frac{\text{Metal Mass}}{\text{Intensity}} \times \frac{NP \text{ Mass}}{\text{Metal Mass}} \times \frac{1}{\text{Polymer Density}}$$

19
20
21
22 The effective spherical NP diameter (d) can then be determined from:
23

$$24 \quad V = \left(\frac{\pi d^3}{6} \right)$$

25
26
27
28 A notable advantage of spICP-MS is its extreme sensitivity. Each NP contributes only a small
29 amount of mass (femtograms) to the suspension. Thus, suspensions of metal-tagged NPs are
30 measurable at part-per-billion mass concentrations. The number of pulses per volume sampled,
31 after accounting for flow rate and TE,⁷⁴ provides PNC. It should be noted that although the NPs
32 are not spherical, no particles of high aspect ratio are formed by cryomilling (Figure 1), thus
33 computation of an equivalent spherical diameter from the spICP-MS analysis does not introduce
34 significant error. Furthermore, as a consequence of the cubic relationship between mass (volume)
35 and size there is a relative insensitivity of the PSD to small uncertainties in the mass loading of the
36 metal.
37
38
39
40
41
42
43
44
45
46
47
48

49
50 To evaluate the ability of spICP-MS to simultaneously discriminate different NPs prepared
51 with different metal tags in a mixture, a suspension containing NPs of PS loaded with
52 zirconium(IV) ethoxide, PMMA loaded with dibutyltin diacetate, and PVP loaded with
53
54
55
56
57
58
59
60

1
2
3 tantalum(V) ethoxide was prepared . To achieve equal amounts (by number density) of the three
4 plastics in suspension, the initial mixture contained 16.5% PMMA , 0.04% PVP, and 83.4% PS by
5 mass. This was necessary to account for the different hydrophobicities of the three polymers.
6
7
8
9

10 **Applications of metal-tagged plastics and nanoplastics in lab-based studies**

11
12 To illustrate the benefits of using metal-tagged plastics and nanoplastics in lab-based
13 studies we conducted demonstrative studies across three environmentally relevant scenarios. In
14 each of these experiments PNC and PSD were determined via spICP-MS.
15
16
17
18

19 **Abrasion:** A PMMA composite loaded with 1% w/w dibutyltin dilaurate was abraded with 320
20 grit sandpaper and particulates formed suspended in DI water.
21
22
23

24 **Photolysis:** A solution of PMMA NPs containing 1 % w/w tantalum (V) ethoxide was irradiated
25 at 300 nm in the presence of 200 mM H₂O₂ for 0, 3, 6, and 12 hours. Additional experimental
26 details are provided in the SI.
27
28
29

30 **Biological uptake:** Developing zebrafish larvae were exposed to suspensions of heterogeneously
31 sized PMMA NPs and tissues collected for metal analysis. Further experimental details are
32 provided in the SI.
33
34
35
36
37
38
39

40 **Results and discussion**

41 **Characterization of metal-tagged plastics and nanoplastics (NPs)**

42
43 We utilized a combination of ATR-IR, DSC, water contact angle, and XPS to ensure that
44 the physiochemical properties of the metal-tagged polymers remain unchanged from the native
45 polymers. ATR-IR assessed the extent to which the addition of the metal tags caused any
46 observable changes in the chemical bonding. There were no observable differences in ATR-IR
47 data for plastics with and without the presence of 1% w/w organometallic additive (Figure SI-2).
48
49
50
51
52
53
54
55
56
57
58
59
60

1
2
3 Similarly, DSC was used to compare the thermal properties of the polymers after introduction of
4 metal tags. Analogous to the ATR-IR data, Figure SI-3-5 indicated no change to the thermal
5 transitions of the plastics with incorporation of 1% w/w organometallic additive.
6
7

8
9
10 Surface chemistry and surface properties are key to determining adsorption, interparticle
11 interactions, and colloidal transport.⁷⁵⁻⁸³ Water contact angle measurements provided a
12 quantitative metric to assess the relative surface hydrophilicity/hydrophobicity of each plastic.^{84,}
13
14
15
16
17 ⁸⁵ As demonstrated in Table SI-2, there were no significant differences in the measured water
18 contact angle for plastics prepared with and without 1% w/w organometallic additive. To further
19 probe the surface properties of the metal-tagged NPs, XPS was used to examine the elemental
20 composition and bonding state of the surface atoms. As demonstrated in Figures SI-6-9, the
21 elemental composition and bonding state of the plastic surface remains unchanged by addition of
22 1% w/w organometallic additives, irrespective of the polymer or the metal additive. Moreover,
23 analysis of the principal metal transitions for each additive (e.g. Ta(4f) for Ta(V) ethoxide)
24 indicated that the metal atom concentration at the surface is below the XPS detection limit
25 (approximately 0.1 at%), consistent with expectations. For example, in the case of PS containing
26 1% w/w Ta(V) ethoxide the calculated at% Ta is approx. 2.6×10^{-4} . These results strongly indicate
27 that the physical and chemical properties of the plastic surface remain unaffected by the
28 introduction of the metal-tags. Therefore, it is reasonable to assume that the interfacial properties
29 of the metal-tagged NPs will be a mirror of the unmodified NPs.
30
31
32
33
34
35
36
37
38
39
40
41
42
43
44
45

46
47 NP sizing using spICP-MS relies on metal additives being distributed relatively uniformly
48 within the composite. μ -X-ray Fluorescence (μ -XRF) mapping of the metal-tagged plastics was
49 used to determine the distribution of metal additive within the polymer matrix. Whereas 1% w/w
50
51
52
53
54 $\text{Sn}(\text{C}_4\text{H}_9)_2(\text{C}_2\text{H}_3\text{O}_2)_2$ PS (Figure 2) and other organometallic complexes produced reasonably
55
56
57
58
59
60

1
2
3 uniformly dispersed metal-tags (Figures SI-10,12-17), the inorganic salt, TaCl₅, was distributed
4
5 heterogeneously in the composite (Figure SI-11), likely a consequence of poor dispersion in the
6
7 PS matrix. This extremely non-uniform dispersion means that the mass of Ta in a given volume of
8
9 PS will be inconsistent and lead to inaccurate measurement of particle size via spICP-MS. Our
10
11 results suggest that organometallic precursors with alkyl ligands are better suited than inorganic
12
13 ligands (i.e. salts) to produce uniform dispersions of metal tags in the majority of polymers.
14
15

16 17 **Quantification and sizing of metal-tagged nanoplastics**

18

19 Single particle optical sensing analysis (SPOS) (Particle Sizing Systems – SNS 760) was
20
21 used to characterize the number and size distribution of colloidal Sn-tagged PS NPs (Figure 4).
22
23 Particle numbers rapidly increase with decreasing size, increasing the probability that submicron
24
25 particles are undercounted and oversized due to multiple particles being present in the measuring
26
27 volume (i.e. coincidence). SPOS analysis shows that 96% of the MPs are less than 5 μm and 60%
28
29 are less than 2 μm in size, although there is a clear instrumental size cut-off for NPs below 700
30
31 nm. This size limitation and lack of particle specificity (all particles generate a signal regardless
32
33 of composition) means that SPOS cannot be used to determine NP number concentrations or size
34
35 distributions in samples that contain NP mixtures or heterogeneous samples that contain other
36
37 types of particles (e.g. water samples containing background natural mineral particles).
38
39
40
41

42 As seen in Figure 5, the size distribution of 1% w/w Ta(OC₂H₅)₃ PMMA NPs are observed
43
44 at sizes between 200 and 700nm with an exponential increase in particle number with decreasing
45
46 size. This distribution has been commonly observed for natural particles⁸⁶ and we propose will
47
48 also reflect the PSD of NPs generated by the environmental weathering of plastic waste. The effect
49
50 on spICP-MS analysis of rapidly increasing particle number with decreasing size has been
51
52 thoroughly explored in a companion study.⁸⁷ Although we have not explicitly explored this aspect,
53
54
55
56
57
58
59
60

1
2
3 other studies have also shown that the PSD of NPs produced from polymers can be tuned by
4
5 varying the conditions of the cryomilling process (i.e. frequency, number, and duration of
6
7 cycles).⁸⁸⁻⁹¹ A potential analytical artifact of our metal-tag approach is the leaching of metal
8
9 additive from the plastic over time when in aqueous suspension, which would manifest itself as a
10
11 particle size distribution and particle number count that decreased over time. However, additive
12
13 leaching rates from plastics are extremely low.⁹²⁻⁹⁵ Consistent with this concept, we have
14
15 experimentally verified that the NP number concentration and size-distribution of these Ta-PMMA
16
17 NPs remains stable in water over the course of six weeks (Figure 5). Given this observation, there
18
19 is no reduction to the metal loading in the NP that would indicate measurable additive leaching
20
21 over this timescale.
22
23
24
25

26
27 There is a lower size limit of metal-tagged NPs that can be detected by spICP-MS as seen
28
29 in Figures 5 and 6. The existence of this limit can be understood by recognizing that in spICP-MS
30
31 each NP is detected as a metal pulse and the sum of these pulse readings is proportional to the
32
33 mass of metal in the NP. The lower limit for NP detection is determined by the smallest individual
34
35 signal associated with a metal-tagged NP that can be distinguished from the background signal
36
37 (see Figure 2). Thus, for NPs below a certain size, the metal pulse generated in the spICP-MS will
38
39 be too small to be discriminated from the background. Undercounting of particle numbers near the
40
41 background can arise due to multiple factors.⁹⁶ The mode, which lies above the limit established
42
43 by sensitivity (vertical lines in Figure 6) can be considered a “practical” lower limit for quantifying
44
45 the PSD of the NPs. As the metal loading increases, this “practical” lower limit will decrease, as
46
47 we observe with the modal size for Ta-PVP quantification decreasing from 0.31 to 0.17 μm as the
48
49 Ta loading increases from 0.1 w/w% to 1 w/w% (Figure 6). It should be noted that increasing the
50
51 metal loading from 0.1 to 1 % only decreases the minimum detectable particle size by a factor of
52
53
54
55
56
57
58
59
60

1
2
3 2.15 due to the cubed relationship between diameter and volume. Similarly, if we were to decrease
4 the threshold size by another factor of approx. 2 this would require increasing the metal loading to
5 10% with an increasing likelihood that some NP physicochemical (e.g. surface) properties will
6 differ from those of the pristine NPs.
7
8
9
10
11

12 The suitability of spICP-MS for sizing NPs is revealed in Figure 7, where the PSD of Ta-
13 PMMA NPs determined by spICP-MS is compared to that obtained by SEM. Both SEM and
14 spICP-MS reveal that NPs are detected almost exclusively below approximately 1 μm and that
15 PNCs exhibit similar exponential decreases between approximately 0.3 – 1.0 μm , the former
16 representing the size threshold for spICP-MS detection of these NPs. As expected, SEM analysis
17 reveals that PNCs continue to increase for particles sizes $< 0.3 \mu\text{m}$. The qualitative agreement in
18 the size distributions measured by spICP-MS and SEM provides strong support for the validity of
19 the steps involved in converting the number concentration of metal pulse areas observed by spICP-
20 MS into the equivalent spherical size distribution.
21
22
23
24
25
26
27
28
29
30
31
32
33
34
35

36 **Alternative NP and MP Labelling Techniques**

37

38 Herein we have described a new method to create labelled polydisperse NPs containing
39 uniformly incorporated metal tags. However, it is important to compare this approach to other
40 recently developed methods for tagging NPs. These tags have either been attached to the NP
41 surface, incorporated into the polymer matrix, or involve the synthesis of a “core-shell” structure.
42
43
44
45
46

47 A relatively straightforward labeling approach is staining the NP via adsorption of a
48 fluorescent dye, such as Nile red.^{37, 38} However, some polymers including polycarbonate,
49 polyurethane, polyethylene terephthalate, and polyvinyl chloride, have been shown to fluoresce
50 only weakly after staining with Nile red, limiting its applicability to lower density (and generally
51
52
53
54
55
56
57
58
59
60

1
2
3 more hydrophobic) plastics.³⁸ Moreover, since the staining is restricted to the NP surface, the
4 fluorophore concentration and thus the fluorescence signal of each particle is limited. The NP
5 surface properties could also be altered by adsorption of the dye. In addition to staining, NPs with
6 embedded fluorescent dyes can be obtained commercially, although these NPs are expensive,
7 typically only obtainable for a limited number of plastics (e.g. PS, PMMA), and generally
8 produced as monodisperse spheres rather than the heterogeneous shapes representative of naturally
9 occurring NPs. Moreover, these NPs are often stabilized in solution by surfactant molecules or
10 have chemically modified surfaces which alter their nascent surface properties. The primary
11 advantage of fluorescent labels is in qualitative tracking of NPs, for example in organism
12 bioaccumulation or exposure/toxicology studies.
13
14
15
16
17
18
19
20
21
22
23
24
25

26 The alternative to fluorescence as a NP labelling strategy has been to incorporate metal
27 tags in a bottom-up synthesis and rely on ICP-MS (or less frequently spICP-MS) as the basis for
28 detection and quantification. For observing NP distribution in matrices such as tissue, the
29 application of ICP-MS is a rapidly expanding field. For example, laser ablation inductively
30 coupled plasma mass spectrometry (LA-ICP-MS) provides in situ elemental mapping^{97,98}, but is a
31 relatively new analytical development and has yet to reach the widespread popularity or appeal of
32 fluorescence microscopy. Some of the advantages of metal-tags over fluorescence-based labelling
33 methods, include tag-stability to photochemical weathering, easy quantification, and a broader
34 range of polymer types that can be labeled. One metal-based labelling approach involves attaching
35 the metal probes (nanoparticles, ions, or hydrophobic organometallic compounds) to the surface
36 of the MPs or NPs through physical adsorption or chemical binding, enabling detection of NPs \leq
37 $2\mu\text{m}$.⁵⁸⁻⁶⁰ However, the use of surface attachment strategies could alter the NPs interactions and
38 therefore environmental behavior. Additionally, labeling particles with metal ions adsorbed to the
39
40
41
42
43
44
45
46
47
48
49
50
51
52
53
54
55
56
57
58
59
60

1
2
3 NP surface has proven challenging as dilution may cause ions to desorb. More stable attachment
4 occurs when positively-charged metallic nanoparticles are coupled with negatively-charged
5 (carboxylate) functional groups on the NP surface through electrostatic interactions, although this
6 approach will almost certainly impact NP surface properties.^{58, 59} While most studies utilize ICP-
7 MS to track the mass concentration of metal-tagged NPs, in principle metal-based surface tags can
8 also serve as a means of sizing NPs using spICP-MS, assuming the amount of tracer present is
9 proportional to the size of the NP. To determine size, both the surface coverage (mass/area) and
10 particle shape must be known and uniform. Validation is difficult for tagging techniques that rely
11 on sorption, as the coverage is usually not quantifiable and desorption of adsorbed tags may occur
12 with changes in concentration, pH, or temperature. Moreover, if some of the metal tags desorb into
13 solution, the size limit for detection by spICP-MS will increase, analogous to an increase in the
14 NP size threshold described in Figure 6.⁶⁰

15
16
17
18
19
20
21
22
23
24
25
26
27
28
29
30
31 A more recent alternative to surface-bound metal tags, has been fabrication of
32 monodisperse NPs with well-defined shapes (usually spherical or sphere like) through the
33 incorporation of metals into the core of the NP, creating a core-shell structure. One of the first
34 metal-tagged NPs generated in this way used a polyacrylonitrile (PAN) core that contained Pd
35 surrounded by a crosslinked polystyrene shell.⁹⁹ Since the Pd atoms are localized within the PAN
36 core rather than adsorbed on the surface of the NP, the surface properties of the polymer remain
37 uncompromised and Pd release unlikely. Additionally, Pd exists at low concentrations in the
38 environment, making it an ideal metal tag for NP detection. The mass recovery of these NPs was
39 quantified by conventional ICP-MS after spiking into complex environmental matrices (e.g.
40 activated sludge before treatment in pilot-scale batch reactors).⁹⁹ Following the initial study, the
41 Pd-containing NPs also found utility in tracking PS NPs in a diverse range of biological and
42
43
44
45
46
47
48
49
50
51
52
53
54
55
56
57
58
59
60

1
2
3 environmental media.^{62, 100-103} This procedure does, however, requires a complex multi-step
4 synthesis where multiple solvents are added in sequence to a reaction vessel, and has not been
5 extended to polymers other than PS. To date, only mono-dispersed approx. 100nm NPs with a
6 smooth or “raspberry-like” morphology have been synthesized. Recently a more complex core
7 shell NP was synthesized via intercalation of metal chloride salts (Au, Pd, or Pt) into a porous
8 core¹⁰⁴ followed by the reduction of the salts to elemental metal. The metal-imbued core was then
9 coated with either PMMA or PS. Metal intensity distributions obtained by spICP-MS analysis
10 indicated a narrow range of mass loadings in all three NP types, but NP size could not be computed
11 from metal mass as the metal only resided in the core and not the shell. Alternatively, Au
12 nanoparticles have been used as a core and coated with a PS, polyacrylic acid copolymer shell to
13 avoid metal salt reduction.³⁹ spICP-MS coupled to field flow fractionation was able to determine
14 the Au nanoparticle loading in each polydisperse NP.
15
16
17
18
19
20
21
22
23
24
25
26
27
28
29

30
31 Size analysis and measurement of PNC of non-tagged NPs is also possible by spICP-MS
32 analysis using ¹³C.⁴⁵ This less abundant isotope of carbon (1.16%) is used to avoid the high natural
33 ¹²C background ICP-MS signal generated by the ubiquitous presence of carbon dioxide. The high
34 ionization potential of carbon (11.26 eV), which causes a low (< 5%) ionization efficiency in the
35 plasma, combined with high carbon background functionally limits ¹³C spICP-MS analysis to sizes
36 above 1.5-2 micron for PS.⁴⁵ Furthermore, the use of ¹³C for NP quantification in complex
37 environmental samples where carbon-containing particles are present is not possible.
38
39
40
41
42
43
44
45
46
47
48

Advantages and Applications of Polydisperse NPs with Uniformly Distributed Metal Tags

49
50
51 The new NP labelling method described herein has a number of advantages compared to
52 existing labelling strategies. For example, this synthetic strategy uses readily available, cheap, pre-
53 synthesized polymers and organometallics as compared to bottom-up polymerization techniques.⁹⁹
54
55
56
57
58
59
60

1
2
3 The solution blending required to generate the metal-tagged plastics is straightforward to
4 implement, making it ideally suited to widespread adoption within different research labs. The
5 method can also be applied to a broad range of polymers which have been detected as NPs in the
6 environment. Specifically, three of the polymers (PE, PS, and PVC) included in our syntheses
7 described in Table 1 account for over 50% of all non-fiber plastics produced.¹ Moreover, the choice
8 of polymer is not limited by its thermal properties, and only requires consideration of polymer and
9 metal-tag solubility when selecting a volatile, organic solvent for preparing composites. Therefore,
10 this method could be extended to metal-tag numerous other natural or synthetic polymers.
11
12
13
14
15
16
17
18
19
20
21

22 For the metal-tagged NPs synthesized by this new method, the entire volume of the NP is
23 used for detection in contrast to other labelling techniques that rely on adsorption⁶⁰, direct
24 attachment⁵⁸⁻⁶⁰, or the presence of metal atoms on the NP surface. Because of this distribution, the
25 metal additives are present at higher concentrations per NP than other labeling methods and yet
26 maintain undetectable surface concentrations. For example, in a 1 μm sized spherical particle, over
27 99% of the metal-tags are more than 1 nm from the surface. As a result, the majority of metal
28 atoms contributing to the spICP-MS signal are contained within the bulk of NP where they do not
29 impact surface properties. This is confirmed by the absence of any difference between water
30 contact angle or ATR-IR spectra observed between metal-tagged and pristine (unmodified)
31 polymers. Since NPs are typically non-porous, PSDs generated by spICP-MS can also estimate
32 geometric surface areas, information that is otherwise extremely difficult to obtain.
33
34
35
36
37
38
39
40
41
42
43
44
45
46

47 To illustrate the range of environmental studies where plastics and polydisperse NPs with
48 uniformly distributed metal-tags can be used effectively we have conducted a number of simple
49 studies. For example, the uniform distribution of the metal-tags throughout the plastics and NPs
50 enables determination of size-dependent concentrations of NPs produced in various transformation
51
52
53
54
55
56
57
58
59
60

1
2
3 processes via spICP-MS, a capability which does not exist for metal core- polymer shell NPs. To
4 demonstrate this ability, we measured the PSDs of NPs generated by physical abrasion of a
5 macroscopic plastic sample. spICP-MS analysis revealed that the abrasion process produced NPs
6 in the 0.3 to 1 μm size range (Figure 8), an approach that could be expanded to quantify both the
7 efficiency and PSD of NPs generated from different polymers under more well controlled abrasion
8 conditions. In this application our synthetic procedure also enables selection of specific metal-tags,
9 notably metals (e.g. Ta, Sn) that not only exhibit high sensitivity in the spICP-MS but are also
10 absent in most environmental matrices. In the context of abrasion studies for example this allows
11 us to discriminate NPs produced from the polymer from natural NPs present in the natural
12 environment or those produced by the abrading material.
13
14
15
16
17
18
19
20
21
22
23
24
25

26 spICP-MS can also follow the size dependent evolution of NPs in response to external
27 stimuli. For example, due to the photostability of the embedded metal tags,¹⁰⁵ spICP-MS analysis
28 can track the size dependent photodegradation of PMMA NPs exposed 300 nm irradiation in the
29 presence of H_2O_2 . spICP-MS analysis showed that the overall NP concentration decreased
30 systematically as a function of increasing irradiation time (Figure 9). Additionally, visual
31 inspection of the data collected at 0 hours and 6 hours demonstrates that there is a greater decrease
32 in the number of NPs < 500 nm as compared to NPs > 900 nm, implicating a size dependent
33 reactivity trend.
34
35
36
37
38
39
40
41
42
43
44

45 Among the most significant experimental advantages of our analytical approach is the
46 ability to use unique metal tags for different NP types. This allows spICP-MS to simultaneously
47 acquire data on the different metals present in mixtures, thereby enabling the PSD and PNC of
48 different polymeric NPs to be determined in a single experiment. For example, in Figure 10 we
49 demonstrate concurrent detection and quantification of PVP tagged with Ta, PMMA tagged with
50
51
52
53
54
55
56
57
58
59
60

1
2
3 Sn and PS tagged with Zr in the same solution via spICP-MS. In this example, the mass of the
4 three polymer composites was varied to create a NP suspension where the observable particle
5 number concentration of PS, PMMA, and PVP NPs was similar. It should be noted that this
6 approach can also be extended to study NPs derived from the same polymer and subjected to
7 different aging conditions (e.g., one metal could be used to tag non-weathered PS NPs, while a
8 different metal could be used to tag photochemically-weathered PS NPs). This can greatly reduce
9 the experimental burden in studies designed to compare and contrast the behavior of NPs in
10 different environments (e.g. soil transport and mesocosm studies), allowing a single experiment to
11 yield data on up to as many as 4-5 different types of NPs while also ensuring that experimental
12 conditions remain constant during data acquisition.
13
14
15
16
17
18
19
20
21
22
23
24
25

26 In addition to the aforementioned applications, the metal-tagged NPs could be utilized in
27 studies designed to measure size-dependent NP uptake and toxicity in biological organisms since
28 their surface properties are unchanged compared to those of the non-labelled NPs and the metal
29 tags are not subject to leaching over the timescale of most biological uptake studies(see Figure
30 5). For example, we have successfully used spICP-MS to quantify the uptake of heterogeneously
31 sized PMMA NPs (tagged with Ta) into developing zebrafish larvae. The PSD of the NP taken
32 up by the zebrafish and the original stock are compared in Figure 11. Particle number in each size
33 bin has been normalized by the total number measured (left axis, Figure 11). Enhanced uptake of
34 the smaller NPs is apparent, evidenced by the increasing ratio of NPs measured in the original
35 stock used to dose the ZF to the NPs extracted from the ZF tissue, plotted as a function of NP size
36 (right axis, Figure 11). Application of metal-tagged NPs in biological uptake studies described
37 here in could be expanded. For example, organic additives typically encountered in polymers (e.g.
38
39
40
41
42
43
44
45
46
47
48
49
50
51
52
53
54
55
56
57
58
59
60

1
2
3 benzophenones) could also be introduced into the casting solution to create more chemically
4
5 complex but realistic NPs.
6

7
8 There are, however, certain scenarios where the presence of the metal tags would likely
9
10 preclude their application, for example, in NP biodegradation studies. It is also important to
11
12 recognize that the method of NP preparation, particularly the use of sonication, may modify a
13
14 polymer's average molecular weight¹⁰⁶⁻¹⁰⁹ and therefore some of its physicochemical (e.g.
15
16 mechanical) properties. Consequently, these altered polymer characteristics should be quantified
17
18 in situations where NP behavior, or release potential is expected to be impacted such as in NP
19
20 release as a result of wear or abrasion.
21
22
23
24
25

26 **Conclusions**

27
28 This study illustrates a new approach to synthesize labelled nanoplastics (NPs) for a wide
29
30 range of polymer types, where the presence of uniformly distributed metal atoms enables counting
31
32 and sizing of polydisperse NPs across a sub-micron size distribution by spICP-MS. This
33
34 information enables us to quantify particle size distributions (PSDs) and particle number
35
36 concentration (PNCs), even when the NPs are present at low μgL^{-1} concentrations. The elemental
37
38 specificity of spICP-MS facilitates analysis in complex, multi-component matrices, which can
39
40 contain background particles that would confuse other particle analysis methods (NTA, DLS).
41
42 Moreover, the flexibility of the synthetic approach allows unique metal tags to be used for different
43
44 NPs (e.g. Ta for PMMA, Sn for PVC) opening up the possibility to quantify the behavior of
45
46 mixtures of polydisperse NPs under the same experimental conditions. In addition to the examples
47
48 discussed, this new analytical approach could be applied to lab-based studies designed to study the
49
50
51
52
53
54
55
56
57
58
59
60

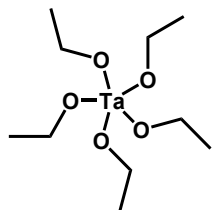
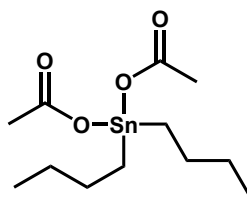
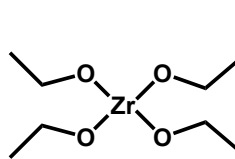
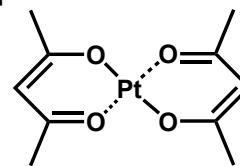
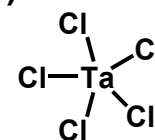
1
2
3 behavior and release potential of NPs in other environmental matrices such as food, drinking water,
4
5 packaging materials, and to assess potential routes of NP human health exposures (e.g. air-borne).
6
7
8
9

10 **Ethical statement**

11
12 All animal procedures were performed in accordance with the Guidelines for Care and Use of
13
14 Laboratory Animals of Texas Tech University and approved by the Animal Ethics Committee
15
16 under protocol number 2022-1281.
17
18
19
20

21 **Acknowledgements**

22
23 This work was partially supported by the National Science Foundation grant # 2003481. The
24
25 authors would like to thank Patrick Eckhert for assistance with SEM imaging, as well as Nasim
26
27 Ganji for assistance performing XPS measurements. μ -XRF scans were performed by the Minerals
28
29 and Materials Characterization Laboratory at the Colorado School of Mines and at the National
30
31 Renewable Energy Laboratory in Golden, CO.
32
33
34
35
36
37
38
39
40
41
42
43
44
45
46
47
48
49
50
51
52
53
54
55
56
57
58
59
60

**Tantalum(V)
Ethoxide****Dibutyltin
diacetate****Zirconium(IV)
ethoxide****Platinum 2,4-
pentanedionate****Tantalum(V)
chloride**

	✓ benzene or THF	✓ THF	✓ benzene	✗ chloroform or THF	✗ chloroform
PS					
	✓ toluene or THF	✓ THF	✗ toluene	✗ toluene	✗ chloroform
PMMA					
	✓ methanol				
PVP					
	✓ toluene				
PE					
	✓ THF	✗ THF			
PVC					

Tables

Table 1: *Combinations of organometallic additive, polymer, and solvent utilized to create metal-tagged NPs to-date. A “check” indicates successful yield of homogenous composite. An “x” indicates a failed composite.*

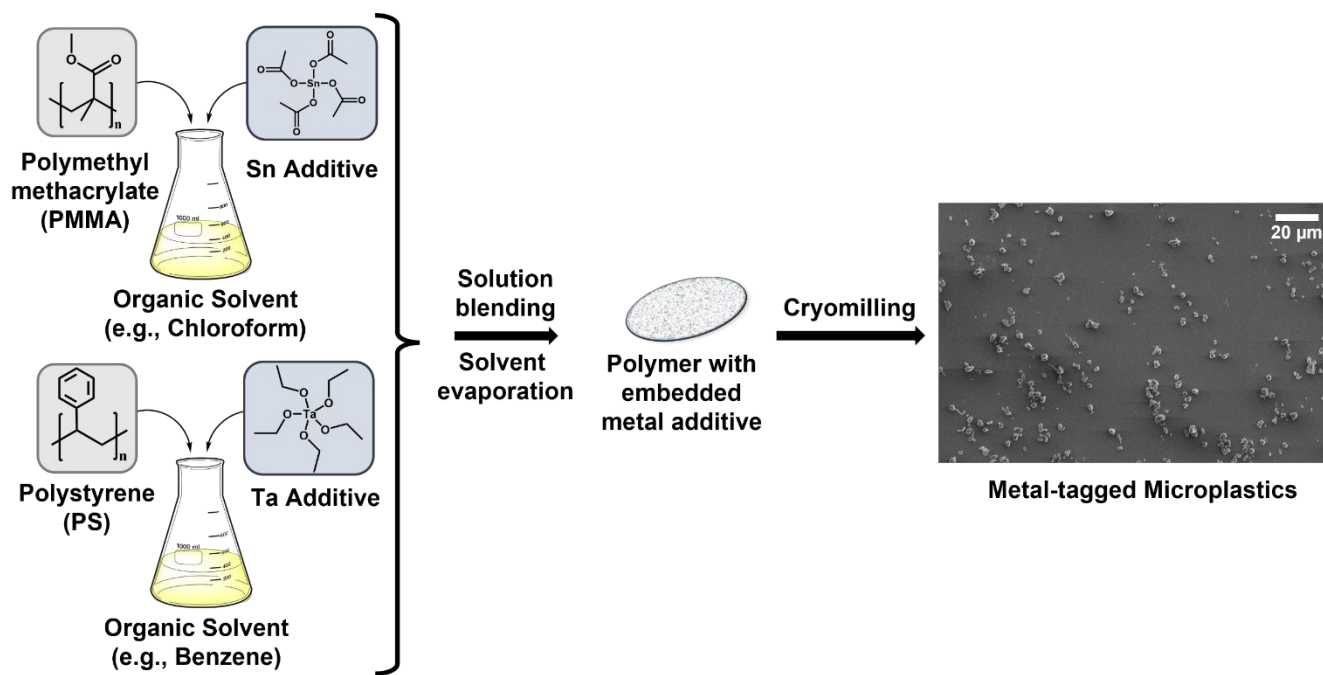
Figures

Figure 1: Synthesis of nanoplastics (NPs) with embedded metal tags. The metal tags are incorporated into the polymer by solution blending before NPs are generated by cryomilling. The SEM image shows an example of colloiddally stable NPs produced in this way (see text for details).

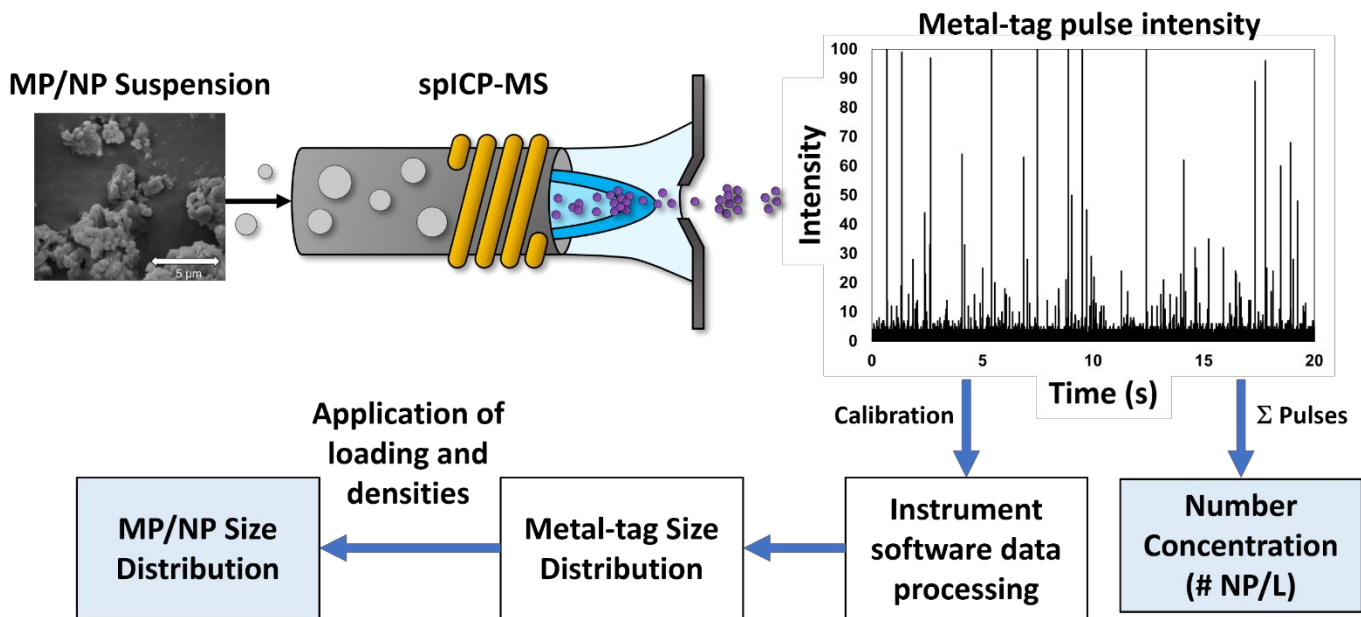


Figure 2: Single-particle ICP-MS quantifies the number concentration, mass concentration and size distribution of $< 1\ \mu\text{m}$ sized metal tagged nanoplastics (NPs).

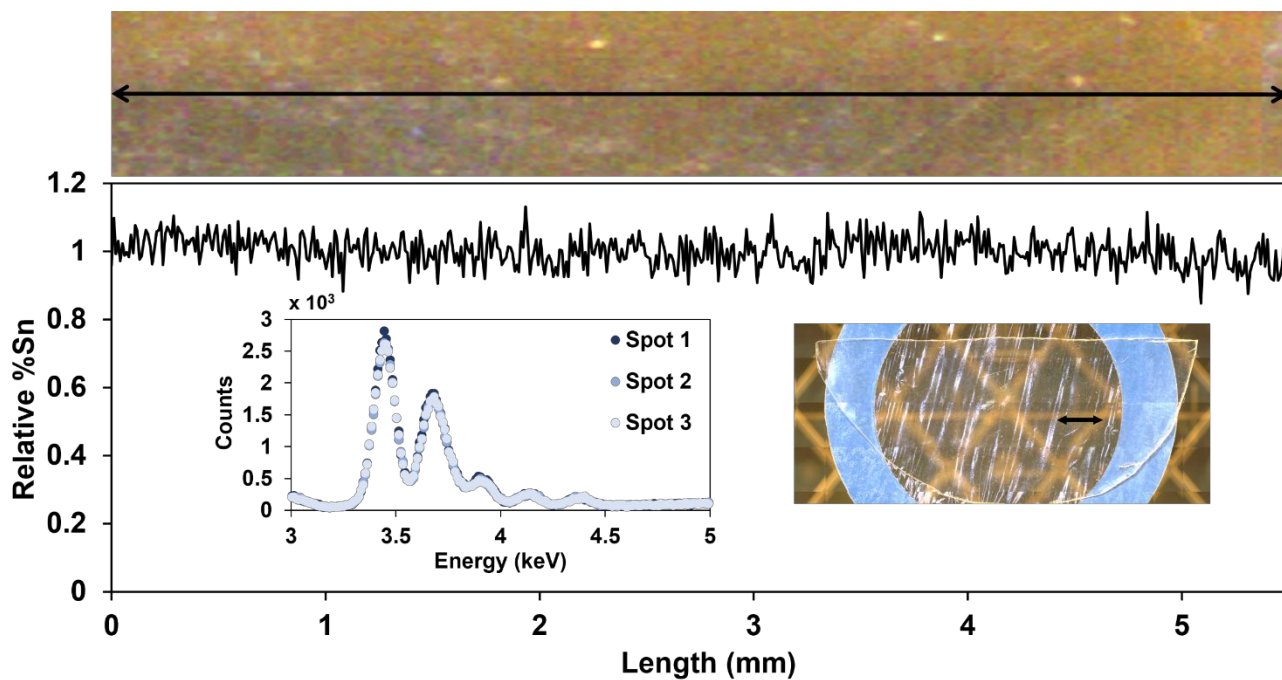


Figure 3: *uXRF* of a 1 w/w % Sn-PS composite. Shown is the relative % Sn detected as a function of composite length to demonstrate the uniformity of metal loading within the plastic. Data collected at a 10 μm spot size over a sample distance of 5 mm.

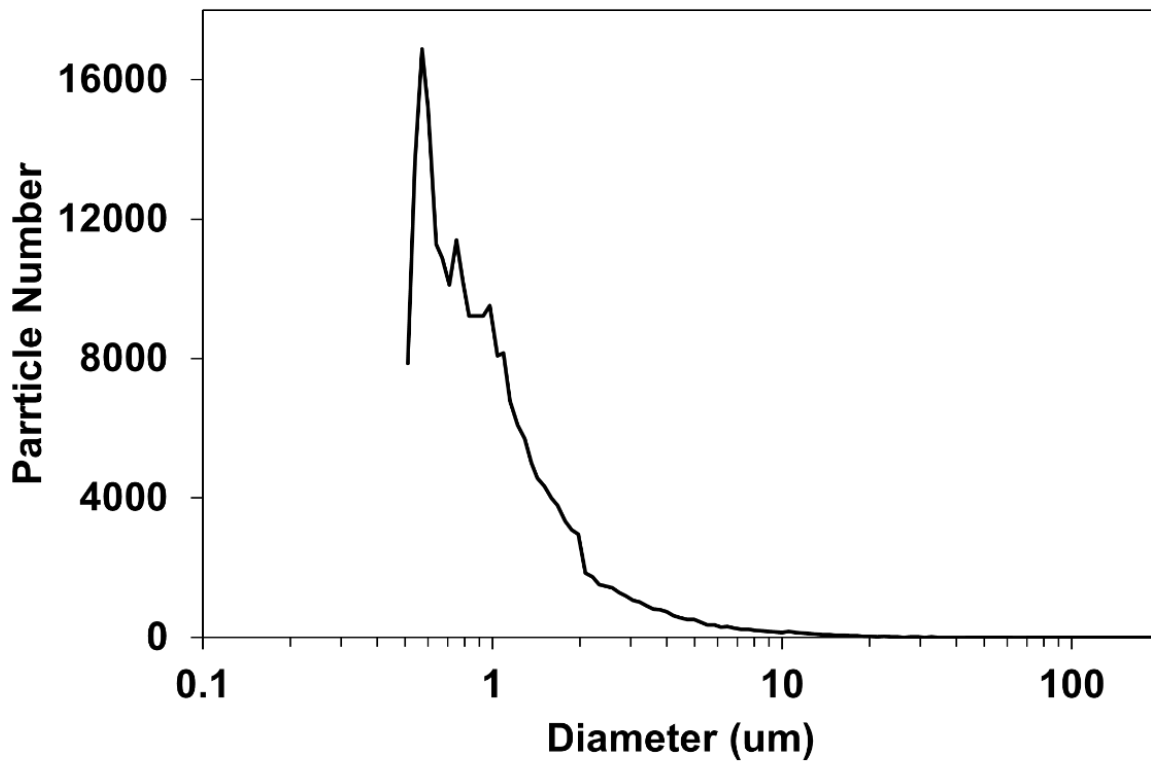


Figure 4: Particle size and number distribution determined by SPOS for a 1 w/w % Sn-PS NP suspension.

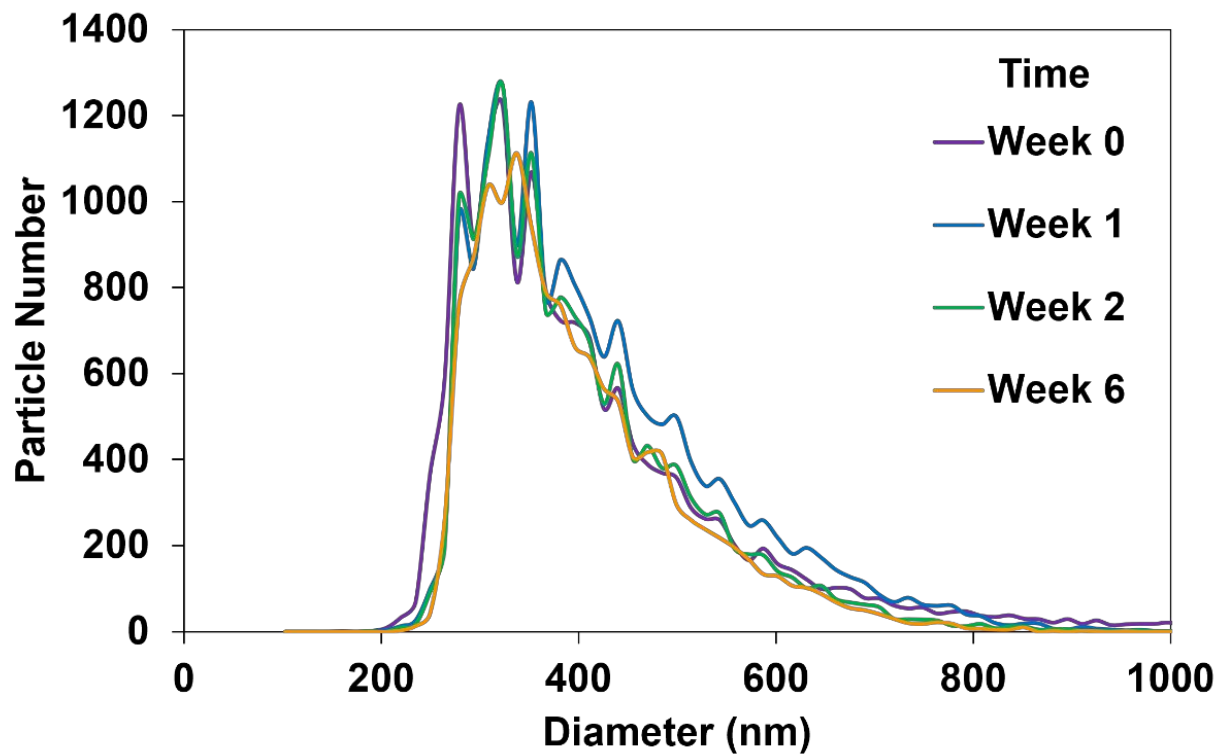


Figure 5: Particle size distribution determined by spICP-MS for a 1 w/w % Ta-PMMA suspension stored in the dark at room temperature and sampled over 6 weeks.

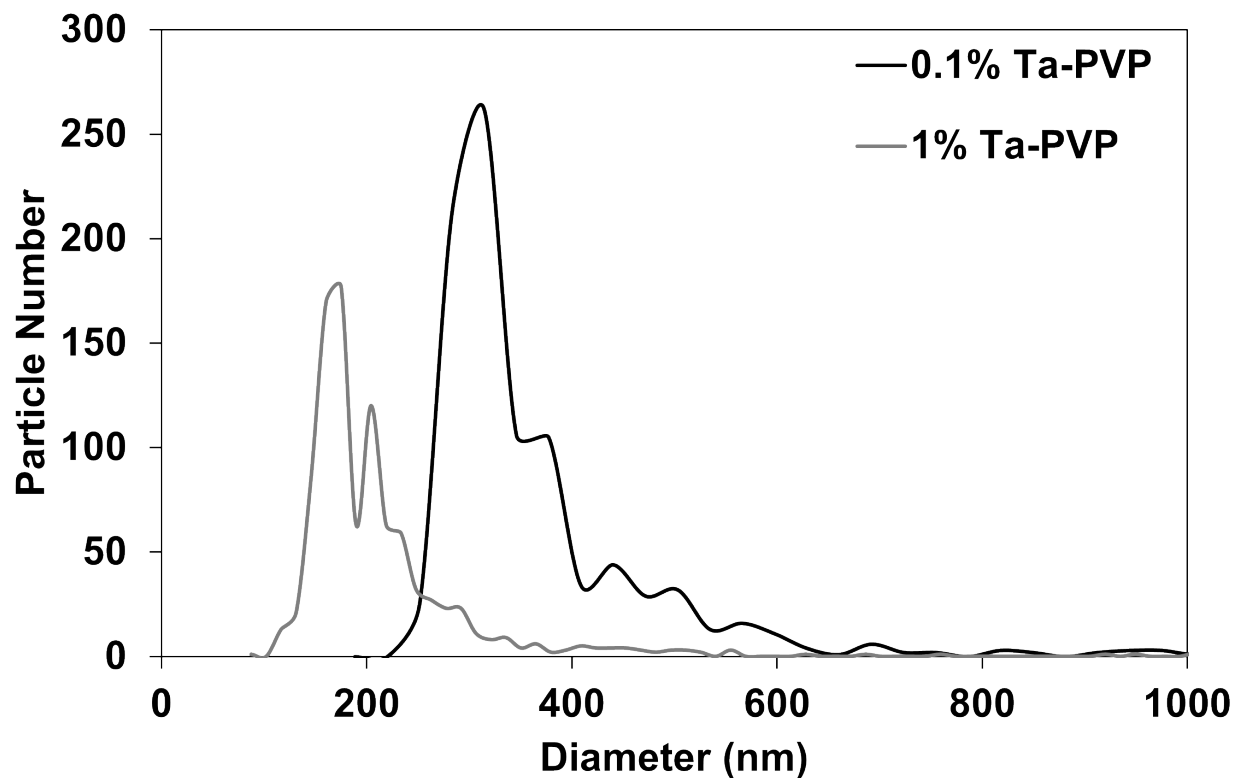


Figure 6: Particle size distributions of 0.1 w/w % Ta-PVP and 1 w/w % Ta-PVP NP suspensions. The minimum NP size measured by spICP-MS is directly affected by the organometallic additive weight % loading.

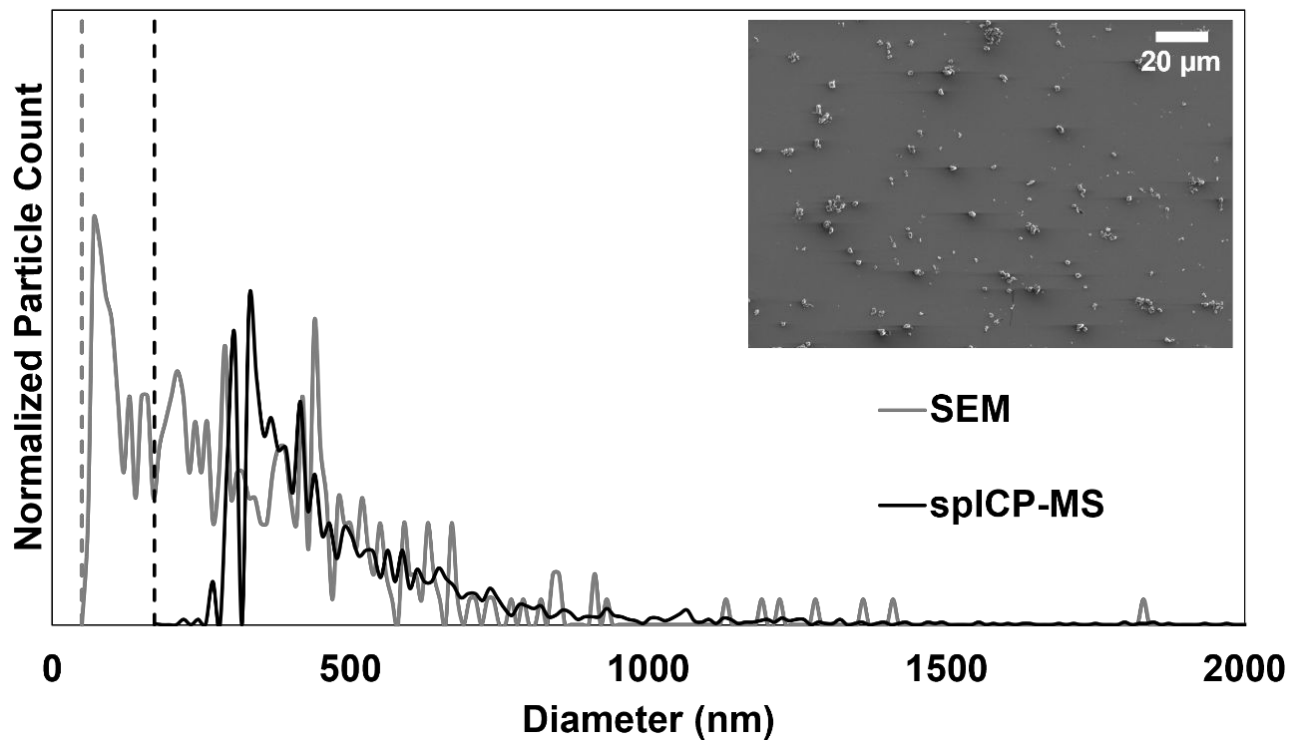


Figure 7: Illustrative comparison of the particle size distribution determined by SEM vs. spICP-MS for the same colloidal suspension sample of 1 w/w % Ta-PMMA NPs. Counts were normalized by the overlapping area (≥ 260 nm diameter); 403 particles were detected by SEM and 3160 by spICP-MS.

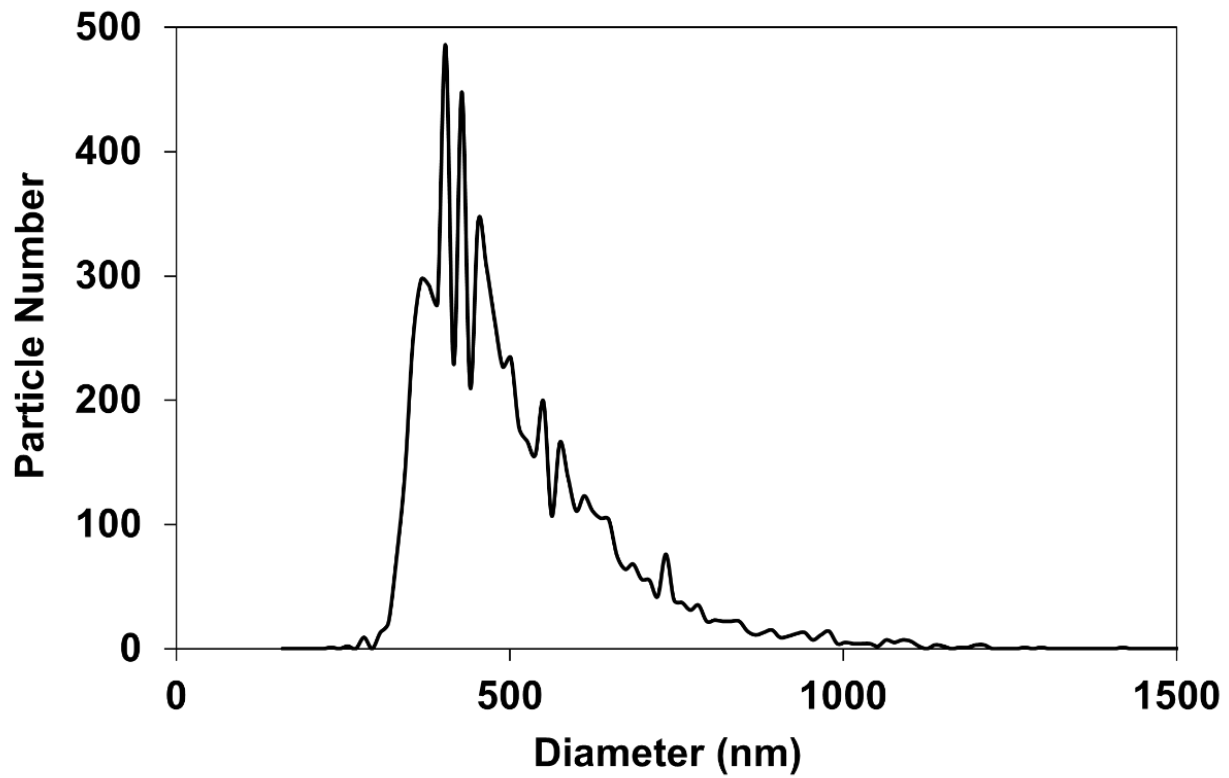


Figure 8: Particle size distribution of 1 w/w % Sn-PMMA NPs generated by physical abrasion of a macroscopic 1 w/w % Sn-PMMA sample.

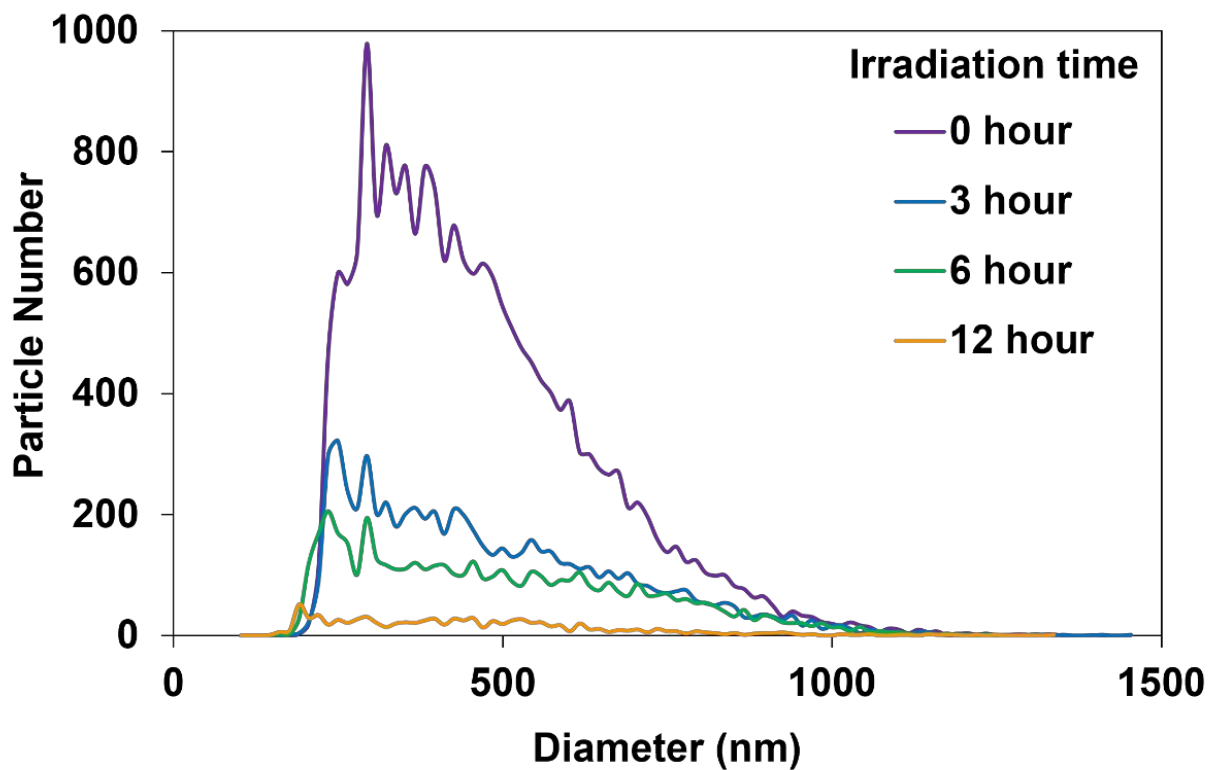


Figure 9: Particle size distributions of a 1 w/w % Ta-PMMA NPs suspension over the course of 12 hours of accelerated photochemical weathering in the presence of 300nm light and 200 mM hydrogen peroxide.

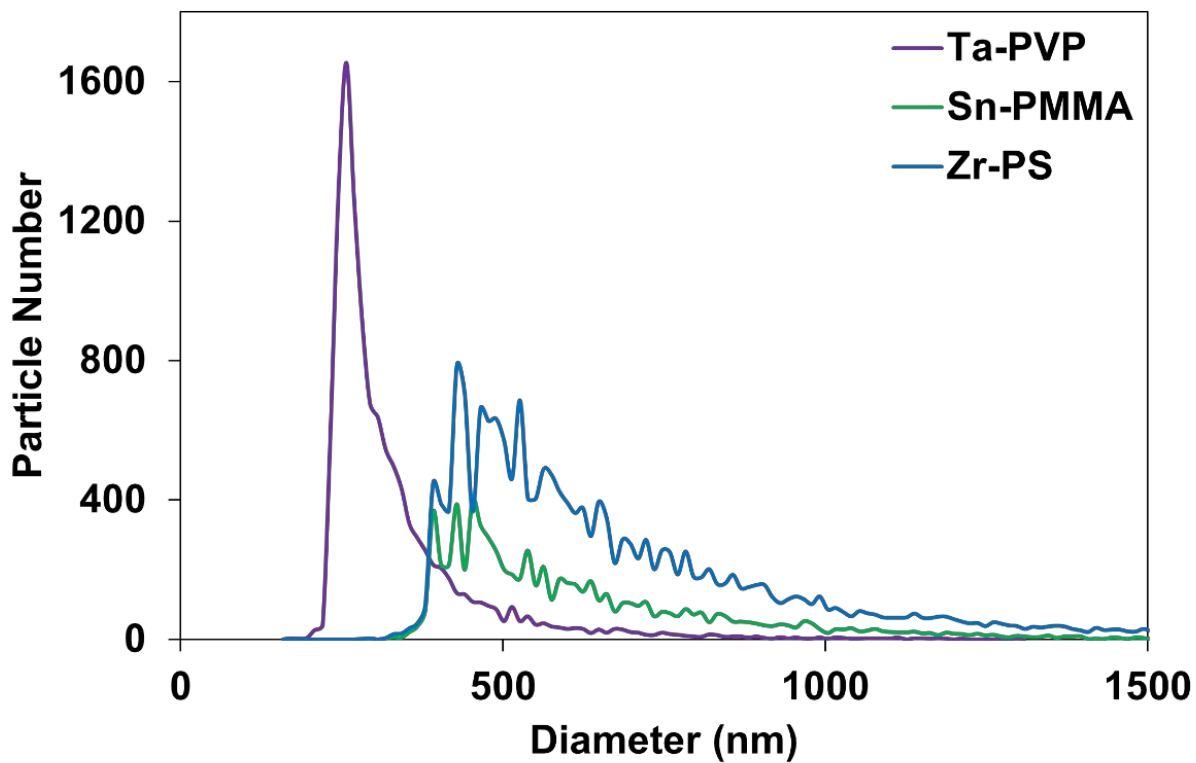


Figure 10: Particle size distributions obtained for a sample containing a mixture of Ta-PVP, Sn-PMMA, and Zr-PS NPs suspended in water of equal amounts (by number density). All microplastics contained 1 w/w % metal loading.

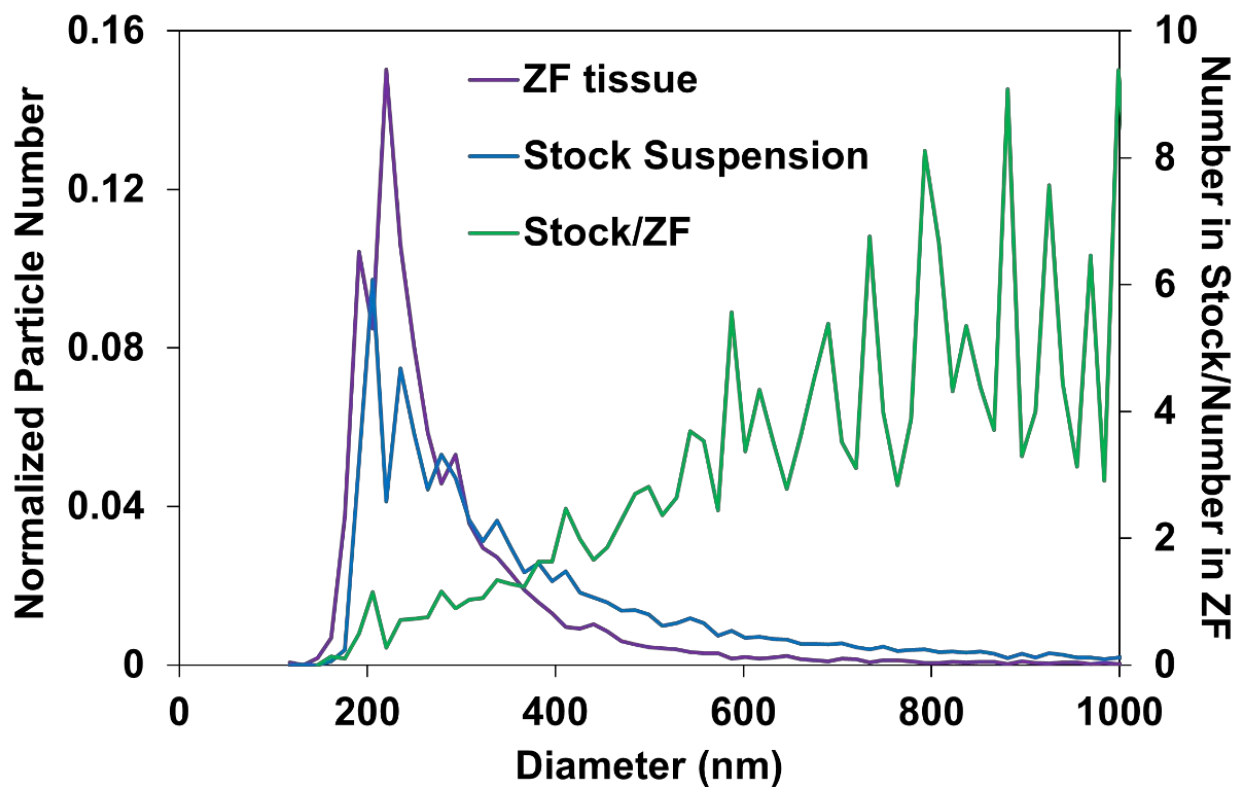


Figure 11: Particle size distributions for PMMA nanoplastics containing 1 w/w % Ta uptaken by zebrafish larvae. Particle numbers are normalized to total number of measured particles. Further experimental details are described in the SI.

References

1. R. Geyer, J. R. Jambeck and K. L. Law, *Science Advances*, 2017, **3**, e1700782.
2. M. W. Ryberg, M. Z. Hauschild, F. Wang, S. Averous-Monnery and A. Laurent, *Resources, Conservation and Recycling*, 2019, **151**, 104459.
3. D. M. Mitrano, P. Wick and B. Nowack, *Nature Nanotechnology*, 2021, **16**, 491-500.
4. J.-P. W. Desforges, M. Galbraith, N. Dangerfield and P. S. Ross, *Marine Pollution Bulletin*, 2014, **79**, 94-99.
5. N. P. Ivleva, A. C. Wiesheu and R. Niessner, *Angewandte Chemie International Edition*, 2017, **56**, 1720-1739.
6. E. Panel o. C. i. t. F. Chain, *EFSA Journal*, 2016, **14**, e04501.
7. K. Betts, *Environmental Science & Technology*, 2008, **42**, 8995-8995.
8. N. B. Hartmann, T. Hüffer, R. C. Thompson, M. Hassellöv, A. Verschoor, A. E. Daugaard, S. Rist, T. Karlsson, N. Brennholt, M. Cole, M. P. Herrling, M. C. Hess, N. P. Ivleva, A. L. Lusher and M. Wagner, *Environmental Science & Technology*, 2019, **53**, 1039-1047.
9. F. Zhu, C. Zhu, C. Wang and C. Gu, *Bulletin of Environmental Contamination and Toxicology*, 2019, **102**, 741-749.
10. J. Li, D. Yang, L. Li, K. Jabeen and H. Shi, *Environmental Pollution*, 2015, **207**, 190-195.
11. M. Cole, P. Lindeque, E. Fileman, C. Halsband, R. Goodhead, J. Moger and T. S. Galloway, *Environmental Science & Technology*, 2013, **47**, 6646-6655.
12. L. C. de Sá, M. Oliveira, F. Ribeiro, T. L. Rocha and M. N. Futter, *Science of The Total Environment*, 2018, **645**, 1029-1039.
13. Y.-L. Wang, Y.-H. Lee, I.-J. Chiu, Y.-F. Lin and H.-W. Chiu, *International Journal of Molecular Sciences*, 2020, **21**, 1727.
14. M. F. M. Santana, F. T. Moreira and A. Turra, *Mar Pollut Bull*, 2017, **121**, 154-159.
15. L. G. A. Barboza, A. Dick Vethaak, B. R. B. O. Lavorante, A.-K. Lundebye and L. Guilhermino, *Marine Pollution Bulletin*, 2018, **133**, 336-348.
16. F. Ribeiro, D. M. Mitrano, C. Hacker, P. Cherek, K. Brigden, S. L. Kaserzon, K. V. Thomas and T. S. Galloway, *Environmental Science & Technology*, 2022, **56**, 16716-16725.
17. E.-L. Ng, E. Huerta Lwanga, S. M. Eldridge, P. Johnston, H.-W. Hu, V. Geissen and D. Chen, *Science of The Total Environment*, 2018, **627**, 1377-1388.
18. S. Lambert and M. Wagner, *Chemosphere*, 2016, **145**, 265-268.
19. *Environmental Science & Technology*, 2017, **51**, 7747-7748.
20. S. Klein, E. Worch and T. P. Knepper, *Environmental Science & Technology*, 2015, **49**, 6070-6076.
21. S. Kühn, A. van Oyen, A. M. Booth, A. Meijboom and J. A. van Franeker, *Chemosphere*, 2018, **213**, 103-113.
22. A. Ter Halle and J. F. Ghiglione, *Environ Sci Technol*, 2021, **55**, 14466-14469.
23. L. Sørensen, E. Rogers, D. Altin, I. Salaberria and A. M. Booth, *Environmental Pollution*, 2020, **258**, 113844.
24. R. E. Engler, *Environmental Science & Technology*, 2012, **46**, 12302-12315.
25. K. Ashton, L. Holmes and A. Turner, *Mar Pollut Bull*, 2010, **60**, 2050-2055.
26. M. Bittelli, G. S. Campbell and M. Flury, *Soil Science Society of America Journal*, 1999, **63**, 782-788.
27. Y. Li, E. Padoan and F. Ajmone-Marsan, *Ecotoxicology and Environmental Safety*, 2021, **209**, 111806.

- 1
 - 2
 - 3
 - 4
 - 5
 - 6
 - 7
 - 8
 - 9
 - 10
 - 11
 - 12
 - 13
 - 14
 - 15
 - 16
 - 17
 - 18
 - 19
 - 20
 - 21
 - 22
 - 23
 - 24
 - 25
 - 26
 - 27
 - 28
 - 29
 - 30
 - 31
 - 32
 - 33
 - 34
 - 35
 - 36
 - 37
 - 38
 - 39
 - 40
 - 41
 - 42
 - 43
 - 44
 - 45
 - 46
 - 47
 - 48
 - 49
 - 50
 - 51
 - 52
 - 53
 - 54
 - 55
 - 56
 - 57
 - 58
 - 59
 - 60
28. T. O. Sokmen, E. Sulukan, M. Turkoglu, A. Baran, M. Ozkaraca and S. B. Ceyhun, *Neurotoxicology*, 2020, **77**, 51-59.
29. M. Sun, R. Ding, Y. Ma, Q. Sun, X. Ren, Z. Sun and J. Duan, *Chemosphere*, 2021, **282**, 131124.
30. M. Torres-Ruiz, A. De la Vieja, M. de Alba Gonzalez, M. Esteban Lopez, A. Castano Calvo and A. I. Canas Portilla, *Sci Total Environ*, 2021, **797**, 149125.
31. H. Cheng, Z. Duan, Y. Wu, Y. Wang, H. Zhang, Y. Shi, H. Zhang, Y. Wei and H. Sun, *Environ Int*, 2022, **161**, 107128.
32. H. M. Dusza, E. A. Katrukha, S. M. Nijmeijer, A. Akhmanova, A. D. Vethaak, D. I. Walker and J. Legler, *Environ Health Perspect*, 2022, **130**, 97006.
33. R. Zhang, M. R. Silic, A. Schaber, O. Wasel, J. L. Freeman and M. S. Sepulveda, *Sci Total Environ*, 2020, **724**, 138065.
34. Z. Wang, T. Lin and W. Chen, *Science of The Total Environment*, 2020, **700**, 134520.
35. M. Pivokonský, L. Pivokonská, K. Novotná, L. Čermáková and M. Klimtová, *Science of The Total Environment*, 2020, **741**, 140236.
36. M. Pivokonsky, L. Cermakova, K. Novotna, P. Peer, T. Cajthaml and V. Janda, *The Science of the total environment*, 2018, **643**, 1644-1651.
37. T. Stanton, M. Johnson, P. Nathanail, R. L. Gomes, T. Needham and A. Burson, *Environmental Science & Technology Letters*, 2019, **6**, 606-611.
38. G. Erni-Cassola, M. I. Gibson, R. C. Thompson and J. A. Christie-Oleza, *Environmental Science & Technology*, 2017, **51**, 13641-13648.
39. A. Barber, S. Kly, M. G. Moffitt, L. Rand and J. F. Ranville, *Environmental Science: Nano*, 2020, **7**, 514-524.
40. M. Mowla, S. Shakiba and S. M. Louie, *Chemical Communications*, 2021, **57**, 12940-12943.
41. H. Fakour, S.-L. Lo, N. T. Yoashi, A. M. Massao, N. N. Lema, F. B. Mkhontfo, P. C. Jomalema, N. S. Jumanne, B. H. Mbuya, J. T. Mtweve and M. Imani, *Agriculture*, 2021, **11**, 330.
42. M. S. Bank, D. M. Mitrano, M. C. Rillig, C. Sze Ki Lin and Y. S. Ok, *Nature Reviews Earth & Environment*, 2022, **3**, 736-737.
43. F. Caputo, R. Vogel, J. Savage, G. Vella, A. Law, G. Della Camera, G. Hannon, B. Peacock, D. Mehn, J. Ponti, O. Geiss, D. Aubert, A. Prina-Mello and L. Calzolari, *J Colloid Interface Sci*, 2021, **588**, 401-417.
44. A. Moraz and F. Breider, *Analytical Chemistry*, 2021, **93**, 14976-14984.
45. F. Laborda, C. Trujillo and R. Lobinski, *Talanta*, 2021, **221**, 121486.
46. A. Prasad, J. R. Lead and M. Baalousha, *Science of The Total Environment*, 2015, **537**, 479-486.
47. S. Kefer, O. Miesbauer and H.-C. Langowski, *Polymers*, 2021, **13**, 2881.
48. G. Balakrishnan, M. Déniel, T. Nicolai, C. Chassenieux and F. Lagarde, *Environmental Science: Nano*, 2019, **6**, 315-324.
49. A. G. Rodríguez-Hernández, J. A. Muñoz-Tabares, J. C. Aguilar-Guzmán and R. Vazquez-Duhalt, *Environmental Science: Nano*, 2019, **6**, 2031-2036.
50. V. C. F. Mosqueira, P. Legrand, H. Pinto-Alphandary, F. Puisieux and G. Barratt, *Journal of Pharmaceutical Sciences*, 2000, **89**, 614-626.
51. N. Kalogerakis, K. Karkanorachaki, G. C. Kalogerakis, E. I. Triantafyllidi, A. D. Gotsis, P. Partsinevelos and F. Fava, *Frontiers in Marine Science*, 2017, **4**.

- 1
2
3 52. Y. K. Song, S. H. Hong, M. Jang, G. M. Han, S. W. Jung and W. J. Shim, *Environmental*
4 *Science & Technology*, 2017, **51**, 4368-4376.
5
6 53. E. von der Esch, M. Lanzinger, A. J. Kohles, C. Schwaferts, J. Weisser, T. Hofmann, K.
7 Glas, M. Elsner and N. P. Ivleva, *Frontiers in Chemistry*, 2020, **8**.
8
9 54. F. Blanco, M. Davranche, F. Fumagalli, G. Ceccone and J. Gigault, *Environmental*
10 *Science: Nano*, 2021, **8**, 3211-3219.
11
12 55. L. Eitzen, S. Paul, U. Braun, K. Altmann, M. Jekel and A. S. Ruhl, *Environmental*
13 *Research*, 2019, **168**, 490-495.
14
15 56. A. Paul, L. Wander, R. Becker, C. Goedecke and U. Braun, *Environmental Science and*
16 *Pollution Research*, 2019, **26**, 7364-7374.
17
18 57. H. El Hadri, J. Gigault, B. Maxit, B. Grassl and S. Reynaud, *NanoImpact*, 2020, **17**,
19 100206.
20
21 58. J. Jiménez-Lamana, L. Marigliano, J. Allouche, B. Grassl, J. Szpunar and S. Reynaud,
22 *Analytical Chemistry*, 2020, **92**, 11664-11672.
23
24 59. Y. Lai, L. Dong, Q. Li, P. Li, Z. Hao, S. Yu and J. Liu, *Environmental Science &*
25 *Technology*, 2021, **55**, 4783-4791.
26
27 60. L. Marigliano, B. Grassl, J. Szpunar, S. Reynaud and J. Jiménez-Lamana, *Molecules*, 2021,
28 **26**, 7093.
29
30 61. A. E. P. del Real, D. M. Mitrano, H. Castillo-Michel, M. Wazne, J. Reyes-Herrera, E.
31 Bortel, B. Hesse, J. Villanova and G. Sarret, *Journal of Hazardous Materials*, 2022, **430**,
32 128356.
33
34 62. A. H. Tophinke, A. Joshi, U. Baier, R. Hufenus and D. M. Mitrano, *Environmental*
35 *Pollution*, 2022, **311**, 119933.
36
37 63. W. J. Shim, Y. K. Song, S. H. Hong and M. Jang, *Marine Pollution Bulletin*, 2016, **113**,
38 469-476.
39
40 64. T. Maes, R. Jessop, N. Wellner, K. Haupt and A. G. Mayes, *Scientific Reports*, 2017, **7**,
41 44501.
42
43 65. S. Piehl, A. Leibner, M. G. J. Löder, R. Dris, C. Bogner and C. Laforsch, *Scientific Reports*,
44 2018, **8**, 17950.
45
46 66. M. Scheurer and M. Bigalke, *Environmental Science & Technology*, 2018, **52**, 3591-3598.
47
48 67. L. Yang, Y. L. Zhang, S. C. Kang, Z. Q. Wang and C. X. Wu, *Science of the Total*
49 *Environment*, 2021, **780**.
50
51 68. M. Moniruzzaman and K. I. Winey, *Macromolecules*, 2006, **39**, 5194-5205.
52
53 69. N. G. Sahoo, S. Rana, J. W. Cho, L. Li and S. H. Chan, *Prog. Polym. Sci.*, 2010, **35**, 837-
54 867.
55
56 70. E. Dal Lago, E. Cagnin, C. Boaretti, M. Roso, A. Lorenzetti and M. Modesti, *Polymers*,
57 2019, **12**.
58
59 71. K. Ke, Y. Wang, X.-Q. Liu, J. Cao, Y. Luo, W. Yang, B.-H. Xie and M.-B. Yang,
60 *Composites Part B: Engineering*, 2012, **43**, 1425-1432.
72. J. C. Foster, I. Akar, M. C. Grocott, A. K. Pearce, R. T. Mathers and R. K. O'Reilly, *ACS*
Macro Letters, 2020, **9**, 1700-1707.
73. M. D. Montaña, H. R. Badiei, S. Bazargan and J. Ranville, *Environmental Science: Nano*,
2014.
74. H. E. Pace, N. J. Rogers, C. Jarolimek, V. A. Coleman, C. P. Higgins and J. F. Ranville,
Analytical Chemistry, 2011, **83**, 9361-9369.

- 1
2
3 75. A. R. Deline, B. P. Frank, C. L. Smith, L. R. Sigmon, A. N. Wallace, M. J. Gallagher, D.
4 G. Goodwin, D. P. Durkin and D. H. Fairbrother, *Chem Rev*, 2020, **120**, 11651-11697.
5 76. J. Yang, J. L. Bitter, B. A. Smith, D. H. Fairbrother and W. P. Ball, *Environ. Sci. Technol.*,
6 2013, **47**, 14034-14043.
7 77. B. Smith, J. Yang, J. Bitter, W. P. Ball and D. H. Fairbrother, *Environ. Sci. Technol.*, 2012,
8 **46**, 12839-12847.
9 78. H.-H. Cho, K. Wepasnick, B. A. Smith, F. K. Bangash, D. H. Fairbrother and W. P. Ball,
10 *Langmuir*, 2010, **26**, 967-981.
11 79. K. L. Chen, B. A. Smith, W. P. Ball and D. H. Fairbrother, *Environ. Chem.*, 2010, **7**, 10-
12 27.
13 80. B. Smith, K. Wepasnick, K. E. Schrote, H.-H. Cho, W. P. Ball and D. H. Fairbrother,
14 *Langmuir*, 2009, **25**, 9767-9776.
15 81. B. Smith, K. Wepasnick, K. E. Schrote, A. R. Bertele, W. P. Ball, C. O'Melia and D. H.
16 Fairbrother, *Environ. Sci. Technol.*, 2009, **43**, 819-825.
17 82. H. Fairbrother, B. Smith, J. Wnuk, K. Wepasnick, W. P. Ball, H. Cho and F. K. Bangash, in
18 *Environmental Nanomaterials*, ed. V. Grassian, John Wiley and Sons, New York, 2008, pp.
19 131-156.
20 83. H.-H. Cho, B. A. Smith, J. D. Wnuk, D. H. Fairbrother and W. P. Ball, *Environmental*
21 *Science & Technology*, 2008, **42**, 2899-2905.
22 84. K.-Y. Law, *The Journal of Physical Chemistry Letters*, 2014, **5**, 686-688.
23 85. K.-Y. Law, 2015, **87**, 759-765.
24 86. M. Filella and J. Buffle, in *Colloids in the Aquatic Environment*, eds. T. F. Tadros and J.
25 Gregory, Elsevier, Oxford, 1993, DOI: [https://doi.org/10.1016/B978-1-85861-038-](https://doi.org/10.1016/B978-1-85861-038-2.50021-8)
26 [2.50021-8](https://doi.org/10.1016/B978-1-85861-038-2.50021-8), pp. 255-273.
27 87. S. G. Bevers, C. Smith, S. Brown, N. Malone, D. H. Fairbrother, A. J. Goodman and J. F.
28 Ranville, *Environmental Science: Nano*, 2023, DOI: 10.1039/D3EN00425B.
29 88. M. Cole, *Scientific Reports*, 2016, **6**, 34519.
30 89. Z. Khodsiani, H. Mansuri and T. Mirian, *Powder Technology*, 2013, **245**, 7-12.
31 90. N. Kumar and K. Biswas, *Journal of Materials Research and Technology*, 2019, **8**, 63-74.
32 91. C. J. McColley, J. A. Nason, B. J. Harper and S. L. Harper, *Microplastics and Nanoplastics*,
33 2023, **3**, 20.
34 92. S. Prager and F. Long, *Journal of the American Chemical Society*, 1951, **73**, 4072-4075.
35 93. J. F. N. Valderrama, K. Baek, F. J. Molina and I. J. Allan, *Environmental Science:*
36 *Processes & Impacts*, 2016, **18**, 87-94.
37 94. A. Reynier, P. Dole, S. Humbel and A. Feigenbaum, *Journal of Applied Polymer Science*,
38 2001, **82**, 2422-2433.
39 95. C. Chen, L. Chen, Y. Yao, F. Artigas, Q. Huang and W. Zhang, *Environmental Science &*
40 *Technology*, 2019, **53**, 10741-10752.
41 96. S. Bevers, C. Smith, S. Brown, N. Malone, D. H. Fairbrother and J. Ranville, *Manuscript*
42 *submitted for publication*, 2023.
43 97. D. Metarapi, M. Šala, K. Vogel-Mikuš, V. S. Šelih and J. T. van Elteren, *Analytical*
44 *Chemistry*, 2019, **91**, 6200-6205.
45 98. M. Wang, L.-N. Zheng, B. Wang, H.-Q. Chen, Y.-L. Zhao, Z.-F. Chai, H. J. Reid, B. L.
46 Sharp and W.-Y. Feng, *Analytical Chemistry*, 2014, **86**, 10252-10256.
47 99. D. M. Mitrano, A. Beltzung, S. Frehland, M. Schmiedgruber, A. Cingolani and F. Schmidt,
48 *Nature Nanotechnology*, 2019, **14**, 362-368.
49
50
51
52
53
54
55
56
57
58
59
60

- 1
2
3 100. N. J. Clark, F. R. Khan, C. Crowther, D. M. Mitrano and R. C. Thompson, *Science of The*
4 *Total Environment*, 2023, **854**, 158765.
5 101. N. J. Clark, F. R. Khan, D. M. Mitrano, D. Boyle and R. C. Thompson, *Environment*
6 *International*, 2022, **159**, 106994.
7 102. W. M. Heinze, D. M. Mitrano, E. Lahive, J. Koestel and G. Cornelis, *Environmental*
8 *Science & Technology*, 2021, **55**, 16423-16433.
9 103. S. Frehland, R. Kaegi, R. Hufenus and D. M. Mitrano, *Water Research*, 2020, **182**, 115860.
10 104. R. J. Rauschendorfer, K. M. Whitham, S. Summer, S. A. Patrick, A. E. Pierce, H. Sefi-Cyr,
11 S. Tadjiki, M. D. Kraft, S. R. Emory, D. A. Rider and M. D. Montaña, *Frontiers in*
12 *Toxicology*, 2021, **3**.
13 105. K. D. Sullivan and V. Gugliada, *Marine Pollution Bulletin*, 2018, **133**, 622-625.
14 106. K. S. Suslick and G. J. Price, *Annual Review of Materials Science*, 1999, **29**, 295-326.
15 107. G. J. Price and P. F. Smith, *Polymer*, 1993, **34**, 4111-4117.
16 108. M. T. Taghizadeh and T. Asadpour, *Ultrasonics Sonochemistry*, 2009, **16**, 280-286.
17 109. M. T. Taghizadeh and A. Bahadori, *Journal of Polymer Research*, 2009, **16**, 545-554.
18
19
20
21
22
23
24
25
26
27
28
29
30
31
32
33
34
35
36
37
38
39
40
41
42
43
44
45
46
47
48
49
50
51
52
53
54
55
56
57
58
59
60